Published by Avanti Publishers

International Journal of Petroleum Technology

ISSN (online): 2409-787X

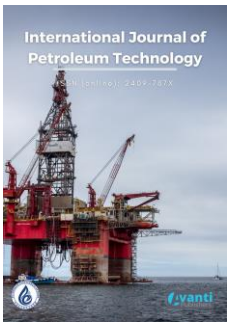

Establishing Time-Depth Relationships Constrained by Modes of the Reservoir Architecture

Huijing Fang[1,2,*], Shubo Yang[3], Guocan Zhang[4] and Huaimin Xu[2]

[1]*Exploration Research Institute, Anhui Provincial Bureau of Coal Geology, Hefei 230088, China*

[2]*College of Geoscience, China University of Petroleum (Beijing), Beijing 102249, China*

[3]*Sinopec Research Institute of Petroleum Engineering, Beijing, 100101, China*

[4]*Sinopec Petroleum Exploration and Production Research Institute, Beijing, 100083, China*

ARTICLE INFO

Article Type: Research Article

Keywords:
Wavelet
Reservoir
Seismic well tie
Architecture mode
Time-depth relationship

Timeline:
Received: January 11, 2022
Accepted: March 22, 2022
Published: April 15, 2022

Citation: Fang H, Yang S, Zhang G, Xu H. Establishing Time-Depth Relationships Constrained by Modes of the Reservoir Architecture. Int J Petrol Technol. 2022; 9: 1-7.

DOI: https://doi.org/10.15377/2409-787X.2022.09.1

ABSTRACT

Time-depth relationships (TDRs) can connect seismic and wireline logs, both essential characterization data of reservoirs. The seismic well tie is always a complex work on account of the complicated reservoir structures. Since seismic and logging data are responses of reservoir architectures, the seismic well tie can be efficiently improved constrained by the reservoir architectures. This study adopts a clastic reservoir as the study area. Three architecture modes (i.e., normal cycle mode, inverse-normal cycle mode, and homogeneous-normal cycle mode) are summarized based on combinations of architecture elements. For the generation of the synthetic seismograms, optimized wavelets (i.e., wavelet A, wavelet B, and wavelet C) are suitable for the wells belonging to normal cycle mode, inverse-normal cycle mode, and homogeneous-normal cycle mode, respectively. Precise TDRs are established by matching the synthetics and seismic traces. Wells belong to the same architecture mode and have similar TDRs. The two-way travel time is shortest in the same depth interval of homogeneous-normal cycle mode compared to other architecture modes.

*Corresponding Author
Email: fanghuijing11@163.com
Tel: +86 15117974129

1. Introduction

Both seismic and wireline logs are essential data for reservoir characterization [1-4]. Seismic data are in the time domain; however, logging data are in the depth domain. Then, it is significant to establish the time-depth relationships (TDRs) between seismic and logging data [5-8]. The seismic well tie is a process of matching the waveform of synthetic seismograms, which is generated from wavelets and reflection coefficients in wells and adjacent seismic traces [9]. To date, researchers propose many approaches to improve the seismic well tie. Cubizolle *et al*. employ a real-time synthetic model to determine the time shift value during the seismic well tie [10]. This method allows checking the global consequences of local change in the TDR. Zhang *et al*. perform the seismic well tie using both synthetic seismogram and impedance log [11]. For every target well, the synthetic seismogram and impedance log are aligned to the nearby trace and inverted impedance, respectively. Wu *et al*. propose a variable-size window resampling algorithm and integrate it with a convolutional neural network to conduct seismic well tie [12]. However, current approaches do not employ geological features in the process of the seismic well tie [13,14]. The seismic data are the responses of reservoir architectures [15,16]. Thus, constrained by the reservoir architectures, the seismic well tie can be efficiently improved.

This study aims to establish precise TDRs constrained by modes of reservoir architecture. A clastic reservoir with abundant seismic and logging data is selected as a study area. Firstly, main architecture elements are analyzed based on cores in the studied interval. Secondly, multiple architecture modes are summarized according to the combination of architectural elements. Thirdly, seismic well ties are conducted by the constrain of architecture modes. Finally, precise TDRs are revealed for the target interval.

For the methodology, we summarize the modes of the reservoir architecture based on vertical lithology sequence. Totally three wells' core description data are analyzed. Moreover, we conduct the match of synthetic seismograms and seismic traces by shifting, stretching, and squeezing the synthetics computed from wireline logs and optimized wavelets. Correction coefficients between synthetic seismograms and seismic traces are employed to evaluate the accuracy of the seismic well tie.

2. Geological Setting

The BX Oilfield, a clastic reservoir in the middle and later stage of development, is selected as the study target. The reservoir is located in the Bohaiwan Basin, an oil-bearing basin in north China [17,18]. Totally 16 vertical wells were drilled in the study area. However, horizontal wells are not used to establish TDR because their two-way travel times in the target zone are limited.

This research focuses on the second parasequence (i.e., IIB parasequence) in the Minghuazhen Formation (Fig. **1**). The burial depth of the IIB ranges from 1120 m to 1280 m, and its average thickness is 102.21 m. Moreover, the IIB corresponds to a fifth-order sedimentary cycle, including three sixth-order sedimentary cycles (i.e., IIB_1–IIB_3 from bottom to top). For the spatial distribution pattern of the sixth-order sedimentary cycles, IIB_2 and IIB_3 are normal steady cycles in the study area. However, inverse and homogeneous cycles are locally developed in the IIB_1.

3. Lithological and Geophysical Properties of Architecture Modes

3.1. Architecture Elements

The IIB is a typical delta front deposit [19,20]. Multiple architecture elements are substantial components of the sedimentary cycles. According to cores and wireline logs analyses, there are eight architecture elements in the IIB (Fig. **2**). As shown in Figs **2a**–**2c**, the distributary channel in IIB contains three kinds of vertical lithology sequences. Besides the general fining-upward sequence (Fig. **2a**), mud with massive stratifications is deposited within the lithology sequence (Fig. **2b**), and conglomeratic siltstone with massive stratifications is sedimented in the bottom of the sequence in some cores (Fig. **2c**). As shown in Figs **2d** and **2e**, the mouth bar in IIB contains two kinds of vertical lithology sequences. One of the sequences contains three lithofacies (i.e., siltstone with trough

stratification, siltstone with horizontal stratification, and fine sandstone with trough stratification from bottom to top, Fig. **2d**), and another is made up of two lithofacies (i.e., argillaceous siltstone with wavy stratification and siltstone with massive stratification, Fig. **2e**). For the interdistributary bay in the IIB, three vertical lithology sequences are observed from cores (Fig. **2f**–**2h**). Besides mud with massive stratifications, siltstone with wavy and massive stratifications acts as thin intervals within the sequence.

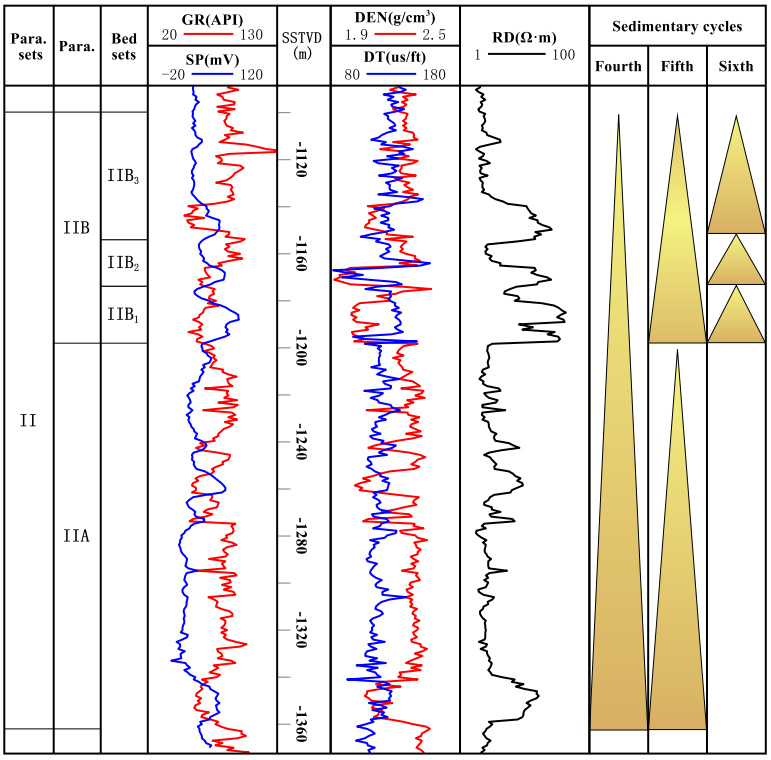

Figure 1: Sequence stratigraphy of well W02 in the study area.

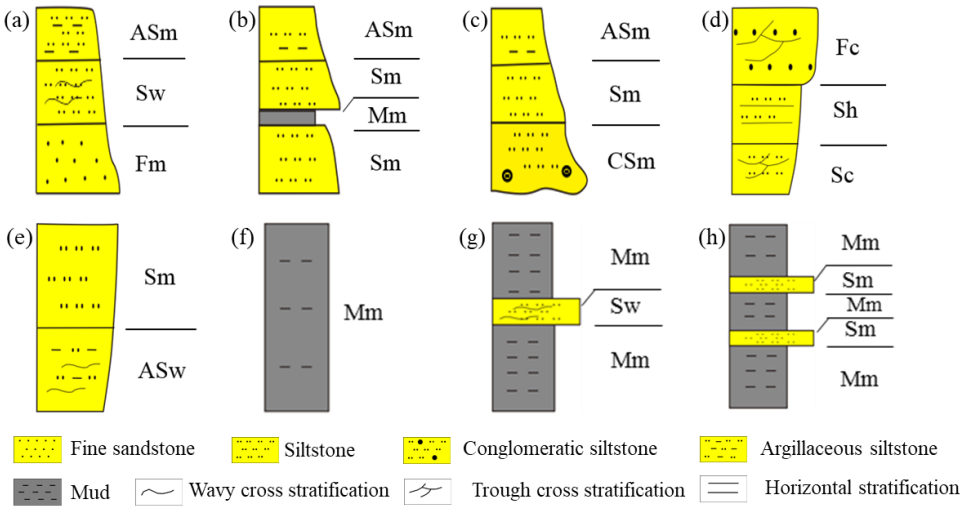

ASm: Argillaceous siltstone with massive stratification; Sw: Siltstone with wavy stratification; Fm: Fine sandstone with massive stratification; Sm: Siltstone with massive stratification; Mm: Mud with massive stratification; CSm: Conglomeratic siltstone with massive stratification; Sc: Siltstone with trough stratification; Sh: Siltstone with horizontal stratification; ASw: Argillaceous siltstone with wavy stratification

Figure 2: Schematic diagrams of (a-c) distributary channel, (d-e) mouth bar, and (f-h) interdistributary bay.

Distributary channels are major architectural elements in the study area. According to the interpretation in wells, the average thicknesses of distributary channels are 16.95 m, 10.31m, and 10.73 m in IIB_1, IIB_2, and IIB_3, respectively.

3.2. Architecture Modes

The vertical combinations of multiple architecture elements are divided into three modes (Fig. 3); normal cycle mode, inverse-normal cycle mode, and homogeneous-normal cycle mode. As shown in Fig. **3a**, every sixth-order cycle in the normal cycle mode is combined by a distributary channel and interdistributary bay. The seismic reflection coefficients get larger and denser from bottom to top in every sixth-order cycle. In the study area, the normal cycle mode is the most common. As shown in Fig. **3b**, the IIB_2 and IIB_3 are combined by distributary channel and interdistributary bay in inverse-normal cycle mode; however, IIB_1 is combined by mouth bar and interdistributary bay. Correspondingly, for inverse-normal cycle mode, the seismic reflection coefficients get smaller and sparser from bottom to top in the IIB_1, and they get larger and denser from bottom to top in the IIB_2 and IIB_3. As shown in Fig. **3c**, the IIB_2 and IIB_3 are combined by distributary channel and interdistributary bay in homogeneous-normal cycle mode; however, IIB_1 is made up of interdistributary bay. Correspondingly, for the homogenous-normal cycle mode, the seismic reflection coefficients are homogenous in the IIB_1, and they get larger and denser from bottom to top in the IIB_2 and IIB_3. Therefore, the architecture modes control the distribution of the seismic reflection coefficients, which directly impact the synthetic pattern during the seismic well tie.

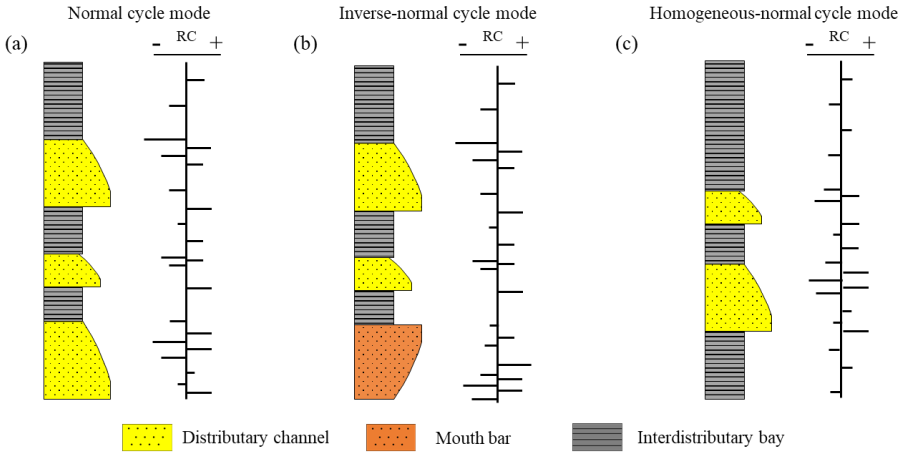

Figure 3: Schematic diagrams of (a) normal cycle mode, (b) inverse-normal cycle mode, and (c) homogeneous-normal cycle mode.

4. Seismic Well Tie and Time-Depth Relationships

4.1. Seismic Well Tie for Multiple Architecture Modes

The seismic well tie for all the vertical wells in the study area is based on the match of synthetics and seismic traces. As shown in Fig. **4a**, well W06 belongs to the normal cycle mode. After seven rounds of comparison, it is found that using wavelet A (Fig. **6a**) can obtain the best synthetic matching the seismic trace adjacent to well W06. The correction coefficient of the synthetic and seismic trace is 0.91 (Fig. **4a**). Well W02 also belongs to the normal cycle mode. When wavelet A is applied for the seismic well tie, the synthetic matches the seismic trace well (Fig. **4b**). Thus, wavelet A is suitable for wells that are in normal cycle mode to conduct seismic well tie.

When wavelet A is applied for well W12 to conduct seismic well tie, the generated synthetic can not match the seismic trace in the lower part (Fig. **5a**). As indicated by the architecture elements combination, the IIB in well W12 belongs to the inverse-normal cycle mode. Then, new wavelets should be extracted from the adjacent seismic trace. After four rounds of comparison, it is found that using wavelet B (Fig. **6b**) can obtain the best synthetic,

matching the seismic trace adjacent to well W12 (Fig. **5b**). Other wells developed the inverse-normal cycle mode can also find good synthetics using wavelet B.

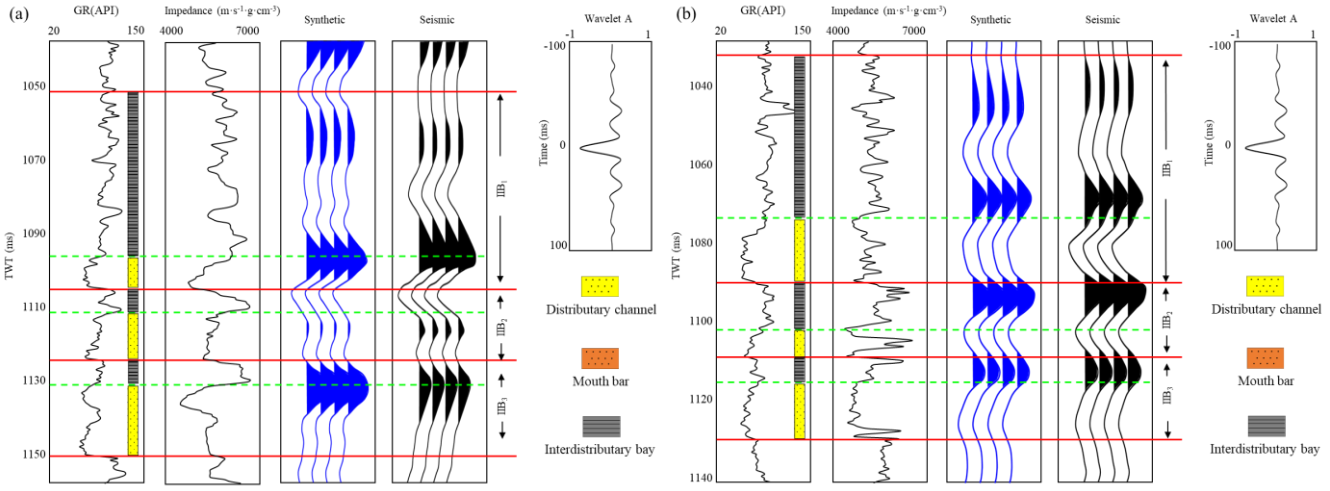

Figure 4: Seismic well tie in well (a) W06 and (b) W02 using wavelet A.

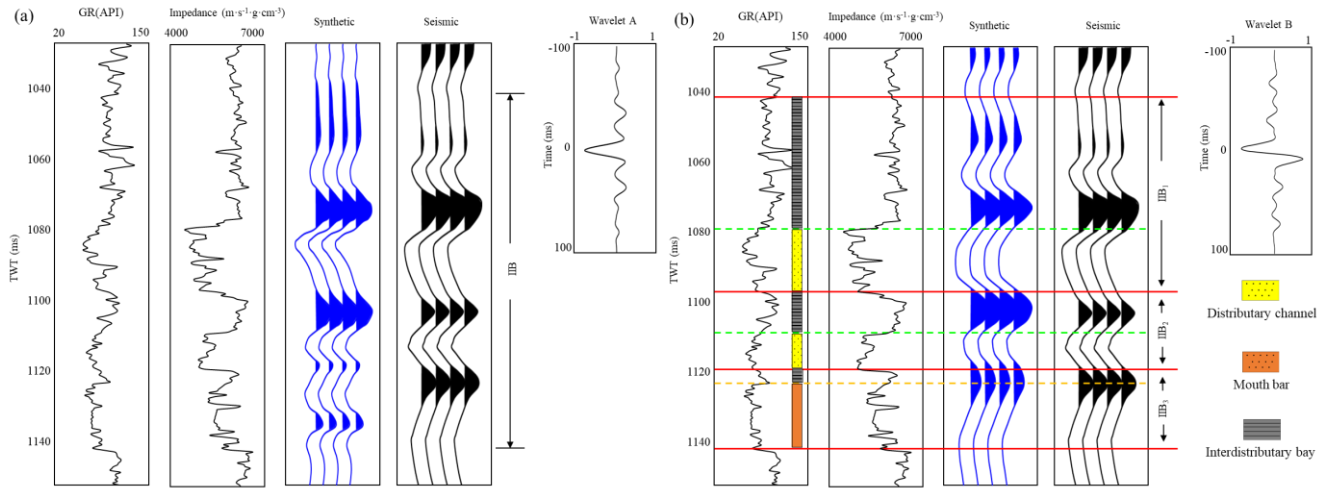

Figure 5: Seismic well tie in well W12 using (a) wavelet A and (b) wavelet B.

Similarly, a new wavelet should be extracted from the seismic trace for wells that belongs to the homogeneous-normal cycle mode. After five rounds of comparison, it is found that wavelet C (Fig. **6c**) is best for seismic well tie of homogeneous-normal cycle mode. Therefore, architecture modes obviously impact the process of the seismic well tie.

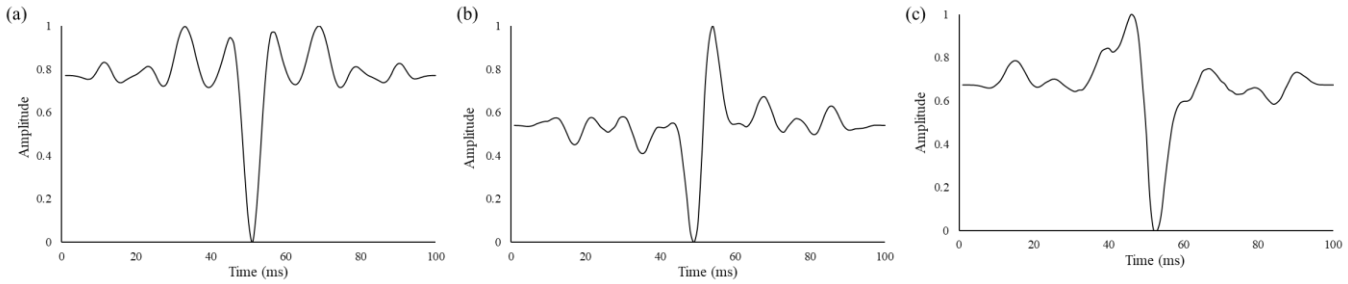

Figure 6: (a) Wavelet A, (b) wavelet B, and (c) wavelet C for the seismic well tie in the study area.

4.2. Time-Depth Relationships Constrained by Architecture Modes

TDR of every well is obtained after seismic well ties. All wells have an approximate linear relationship between two-way travel time (TWT) and depth. However, wells that belong to the same architecture mode have similar TDRs. As shown in Fig. **6a**, solid lines represent the TDRs for the normal cycle modes. Well W11 is a typical well that belongs to the normal cycle modes; the TWT is the longest in the same depth interval compared to other architecture modes (Fig. **6b**). Dotted lines represent the TDRs for the homogenous-normal cycle modes. For well W16, which is a typical well that belongs to the homogenous-normal cycle modes, the TWT is shortest in the same depth interval compared to other architecture modes (Fig. **6b**).

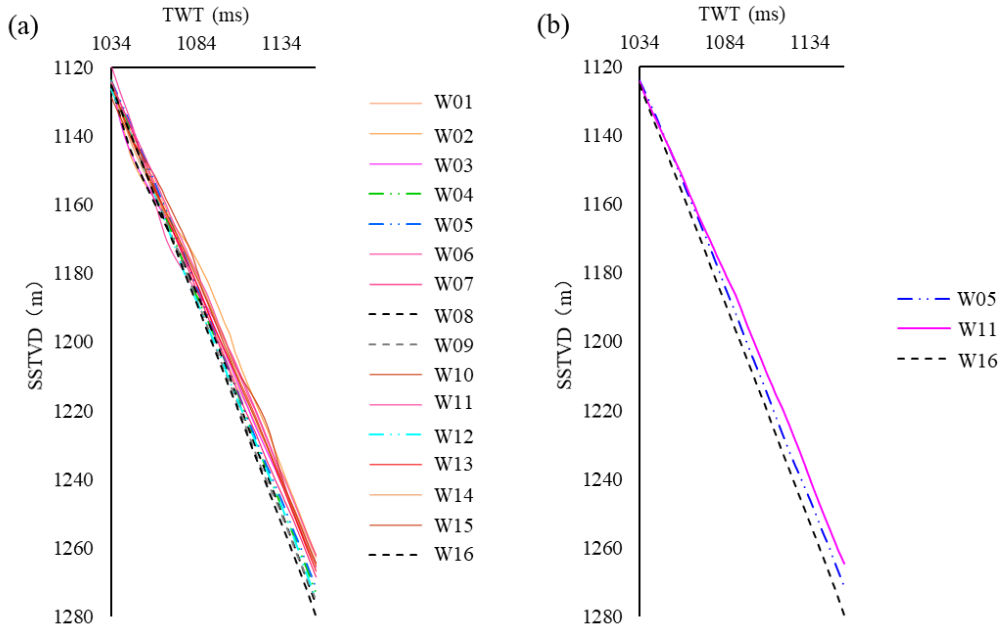

Figure 7: Time-depth relationship of (a) every well and (b) architecture mode in the study area.

5. Conclusions

This study establishes the TDRs for a fifth-order cycle constrained by modes of the reservoir architecture, and specific conclusions are summarized as follows:

a. Three modes of architecture element combinations are developed in the study interval. They are normal cycle mode, inverse-normal cycle mode, and homogeneous-normal cycle mode, respectively.

b. Multiple wavelets are applied for the seismic well tie in the study interval. Wavelet A, wavelet B, and wavelet C are suitable for the wells belonging to normal cycle mode, inverse-normal cycle mode, and homogeneous-normal cycle mode, respectively.

c. Wells belong to the same architecture mode have similar TDRs. The TWT is shortest in the same depth interval of homogeneous-normal cycle mode compared to other architecture modes.

Acknowledgments

This research was supported by the Public Beneficial Geological Project (NO. 2021-g-2-14) in Anhui, China. We are also grateful to the reviewers and editors for their comments and suggestions about this paper.

References

[1] Wagoner J, Mitchum R, Campion K, Rahmanian V. Siliciclastic sequence stratigraphy in well logs, cores, and outcrops: concepts for high-resolution correlation of time and facies. AAPG Special Volumes, 1990; 3-55. https://doi.org/10.1306/Mth7510

[2] Wu X, Shi Y, Fomel S. Incremental correlation of multiple well logs following geologically optimal neighbors. Interpretation, 2018; 6(3): T713-T722. https://doi.org/10.1190/INT-2018-0020.1

[3] Li W, Yue D, Colombera L, Wu S. A novel method for estimating sandbody compaction in fluvial successions. Sedimentary Geology, 2020; 404. https://doi.org/10.1016/j.sedgeo.2020.105675

[4] Bi Z, Wu X, Li Y, Yan S, Zhang S, Si H. Geological-time-based interpolation of borehole data for building high-resolution models: methods and applications. Geophysics, 2022; 87(3): A165-A176. https://doi.org/10.1190/geo2021-0340.1

[5] Smith T, Waterman M. New stratigraphic correlation techniques. The Journal of Geology, 1980; 451-457. https://doi.org/10.1086/628528

[6] Scott W, Leaney P, Ulrych T. Multiple dynamic matching: a new approach to well log correlation[J]. Geoexploration, 1987; 24(6): 503-515. https://doi.org/10.1016/0016-7142(87)90018-4

[7] Wheeler L, Dave H. Simultaneous correlation of multiple well logs. Society of Exploration Geophysicists International Exposition and 84th Annual Meeting SEG, 2014; 618-622. https://doi.org/10.1190/segam2014-0227.1

[8] Muñoz A, Dave H. Automatic simultaneous multiple well ties. Geophysics, 2015; 80(5): IM45-IM51. https://doi.org/10.1190/geo2014-0449.1

[9] Herrera R, Baan M. A semiautomatic method to tie well logs to seismic data. Geophysics, 2014; 79(3): V47-V54. https://doi.org/10.1190/geo2013-0248.1

[10] Cubizolle F, Valding T, Lacaze S, Pauget F. Global method for seismic-well tie based on real time synthetic model. SEG Technical Program Expanded Abstracts, 2015. https://doi.org/10.1190/segam2015-5862834.1

[11] Zhang B, Yang Y, Pan Y, Wu H, Cao D. Seismic well tie by aligning impedance log with inverted impedance from seismic data. Interpretation, 2020; 8: T917-T925. https://doi.org/10.1190/INT-2019-0289.1

[12] Wu H, Li Z, Liu N, Zhang B. Improved seismic well tie by integrating variable-size window resampling with well-tie net. Journal of Petroleum Science and Engineering, 2022; 208. https://doi.org/10.1016/j.petrol.2021.109368

[13] Hornby B, Howie J, Ince D. Anisotropy correction for deviated-well sonic logs: Application to seismic well tie. Geophysics, 2003; 68(2): 464-471. https://doi.org/10.1190/1.1567212

[14] Behiry M, Araby M, Ragab R. Impact of phase rotation on reservoir characterization and implementation of seismic well tie technique for calibration offshore Nile Delta, Egypt. The leading edge, 2022; 39: 346-352. https://doi.org/10.1190/tle39050346.1

[15] Bosch M, Mukerji T, Gonzalez E. Seismic inversion for reservoir properties combining statistical rock physics and geostatistics: A review. Geophysics, 2010; 75(5): 1-53. https://doi.org/10.1190/1.3478209

[16] Shahin A, Tatham R, Stoffa P, Spikes K. Optimal dynamic rock-fluid physics template validated by petroelastic reservoir modeling. Geophysics, 2011; 76(6): O45-O58. https://doi.org/10.1190/geo2010-0275.1

[17] Liu H, Xia Q, Zhou X. Geologic-seismic models, prediction of shallow water lacustrine delta sandbody and hydrocarbon potential in the Late Miocene, Huanghekou Sag, Bohai Bay Basin, northern China. Journal of Palaeogeography, 2018; 7(1): 66-87. https://doi.org/10.1016/j.jop.2017.11.001

[18] Wang M, Xie J, Zhang Q, Duan Y. Characteristics and sedimentary model of a reticular shallow water delta with distributary channels: lower member of the Neogene Minghuazhen Formation in the Bozhong area of the Huanghekou Sag, China. Arabian Journal of Geosciences, 2019; 12(24): 1-21. https://doi.org/10.1007/s12517-019-4928-5

[19] Tian L, Niu C, Du X, Yang B, Lan X, Chen D. Development characteristics and controlling factor analysis of the Neogene Minghuazhen Formation shallow water delta in Huanghekou area. Journal of Paleogeography, 2019; 8(19): 1-19. https://doi.org/10.1186/s42501-019-0032-8

[20] Hao S, Liu H, Du X, Niu C, Sedimentary characteristics of shallow-water delta and responses features in palaeoenvironment: a case study from the lower part of Neogene Minghuazhen Formation. Arabian Journal of Geosciences, 2020; 14: 1-16. https://doi.org/10.1007/s12517-021-06572-y